Copyright © 1997, American Institute of Aeronautics and Astronautics, Inc.

A97-31701 AIAA-97-2211

UNSTEADY AERODYNAMICS OF A CHINED FOREBODY UNDERGOING FORCED PITCH OSCILLATIONS

R. L. Mange*
Lockheed Martin Tactical Aircraft Systems
and
M. B. Bragg**
University of Illinois at Urbana-Champaign

ABSTRACT

A low-speed experimental study of the effects of an oscillatory pitching motion on the flowfield of a chined forebody has been performed. These tests were conducted in the University of Illinois low-speed (0-240 ft/sec), low-turbulence (<0.1%), 3 by 4 ft, open circuit wind tunnel. The high fidelity, NC machined aluminum model was sting mounted and oscillated sinusoidally in pitch from 0° to 52° angle of attack without sideslip. The effects of reduced frequency were investigated by running a range of model oscillation frequency at a nominal Reynolds number, based on the 3-inch base diameter of the forebody, of 2.8×10^5. The experiments cover a range of oscillation frequencies from 0 to 1 Hz, corresponding to reduced frequencies, based on the 10.5-inch length, of 0 to 0.0137. Surface pressures were measured at all conditions using an array of 91 static pressure taps. Normal force and pitching moment were determined by integrating these data. Surface oil and smoke flow visualization were utilized to determine the vortex system and help interpret the surface pressure data.

Steady flow visualization revealed the importance of secondary boundary-layer separation on the leeward surface of the chined forebody. This separation was caused by a steep spanwise surface pressure gradient between the chine edge and the suction pressure peak associated with the primary vortex. Surface static pressure data indicated a hysteresis effect in the unsteady flowfield. Leeward surface static suction pressures built-up at lower angles-of-attack in the dynamic upstroke than in the steady case. The opposite was true in the dynamic downstroke. This hysteresis in leeward surface static pressures also resulted in a hysteresis in secondary boundary-layer separation, secondary vortex formation and the integrated forces and moments. These data showed increased lift in the upstroke and decreased lift in the downstroke, with negligible effects on the center-of-pressure.

INTRODUCTION

Chined forebodies first appeared on production aircraft in 1963 with the first flight of the Lockheed A-12 reconnaissance aircraft. Later versions of this aircraft included the YF-12 interceptor, the D-21 reconnaissance drone and eventually the well known SR-71 reconnaissance aircraft. These aircraft utilized a chined forebody because the chined edges presented an oblique angle to incoming radar waves, thereby drastically reducing the aircraft's radar cross-section (RCS). The highly blended nature of this particular forebody was also suitable for high-speed performance. This combination of reduced RCS and high-speed capability was essential for the type of mission these aircraft were designed to perform.

Another variation of the chined forebody appeared in 1977 with the first flight of the Have Blue prototype. This aircraft, which later evolved into the F-117 stealth fighter, utilized a chined forebody with faceted edges. This forebody also presented an oblique angle to incoming radar waves, but lacked the extremely high speed capability of the blended type of chined forebody used on the SR-71.

Because of the magnitude of the signature reductions being achieved by these production aircraft, and numerous developmental aircraft, much of the data associated with chined forebodies was highly classified. Declassification of reduced RCS shaping technology began in 1989 with the first flight of the B-2 and the first release of F-117 photographs. By 1990, the first flight of the ATF prototypes was complete and reduced RCS shaping technology was becoming increasingly public. By 1994, formal declassification of shaping technology was essentially complete, and unclassified basic research on the steady aerodynamics of these types of shapes was being conducted. However, the application of chined forebodies on fighter aircraft also makes the study of unsteady phenomena important.

* Specialist Senior, Aerodynamics Department, Member AIAA
** Professor, Department of Aeronautical and Astronautical Engineering, Associate Fellow AIAA

Copyright © 1997 by R. L. Mange and M. B. Bragg. Published by the American Institute of Aeronautics and Astronautics, Inc. with permission.

Copyright © 1997, American Institute of Aeronautics and Astronautics, Inc.

Researchers have explored the unsteady aerodynamics of fully three-dimensional configurations that included forebodies, wings, and tails. Of primary interest have been strake-wing[1] and LEX-wing[2] geometries, which represent F-16 and F/A-18 aircraft respectively. The rapid maneuvering, which is required for these modern combat aircraft, results in highly unsteady flowfields which are far more complex than the steady flowfields because they are not only a function of time, but are also dependent on the entire history of the aircraft motion. Rapid pitching motion has been of particular interest because it is regularly encountered in flight, and is beneficial to both lift curve slope and maximum achievable lift.

The effects of pitching motion on a vortex dominated flowfield, such as that of a chined forebody, are pronounced. Numerous studies of the unsteady aerodynamics of highly swept delta wings and strake/wing configurations suggest that a leeward vortex flowfield is significantly altered by rapid pitching motion.[3] This research indicates that vortex lift increases during a dynamic upstroke in angle-of-attack due to a closer coupling between the vortex and the body surface. Vortex breakdown location can also be significantly affected by rapid pitching motion. These changes in the flowfield cause corresponding changes in the leeward surface static pressures.

Recent research on bodies of revolution at angle-of-attack[4] indicate that windward surface pressures are also affected by pitching motion. The pressures on the windward surface of a prolate spheroid are higher during a rapid pitch-up than during the static case. This increased pressure results in higher lift also being generated by the windward surface. These unsteady phenomena on both the windward and leeward surfaced result in a significant change in aerodynamic forces and moments, and therefore can alter an aircraft's performance.[2]

In order to determine the effect of an oscillatory pitching motion on the aerodynamics of a chined forebody, a detailed knowledge of the steady aerodynamics was required. This research provides a better understanding of the steady vortex flowfield through the addition of steady surface and off-body flow visualization data. More complete surface static pressure test data were also obtained to augment the existing force and moment data.[5] This completed database was analyzed to establish the relationships between steady surface static pressures, forces, moments and the vortex flowfield. These relationships served as a basis for the unsteady research and assisted in the analysis of the unsteady data.

Previous studies demonstrate that low flow velocities can contribute significantly to errors in pressure data accuracy.[6] For this reason, this research was conducted primarily at the highest practical flow velocity available (200 ft/sec). In addition, existing research indicates that a significant amount of the unsteady phenomena associated with leeward vortical flowfields occur at low values of reduced frequency. During this research, model oscillation frequencies were held to a maximum of 1.0 Hz, which provided a range of reduced frequencies that are practical to modern fighter aircraft while ensuring good pressure data acquisition system frequency response.

The purpose of this research was to determine the effects of unsteady motion on an important component of a modern high-performance aircraft. A limited amount of published data on the steady flowfield about a chined forebody does exist, however, no results are available in the open literature on the aerodynamics of chined forebodies undergoing forced pitch oscillations. This research will begin to fill the gap between steady chined forebody research and existing unsteady research on related configurations. These data can also be used, in conjunction with current research being conducted in the area of vortex manipulation, to explore methods to improve controllability at high angles-of-attack.

EXPERIMENTAL PROCEDURE

The wind tunnel testing phase of this research was conducted at the University of Illinois, Department of Aeronautical and Astronautical Engineering's subsonic aerodynamics laboratory. An overview of the experimental equipment and procedures used in this research is given in this section. A more detailed description may be found in Mange.[7]

This experimental investigation was conducted in an open circuit wind tunnel, capable of speeds up to 240 ft/sec at a Reynolds number of 1.5×10^6 per foot. The test section is approximately 2.8 feet high, 4.0 feet wide and 8.0 feet long. Windows exist on the tunnel top and sides which provide good visibility and aid in obtaining flow visualization images.

The wind tunnel model, pictured in Figure 1, is a high fidelity, NC machined aluminum chined forebody model. The model is 10.5 inches long with a 3 inch base width. The planform is that of a 3.5 caliber tangent ogive and the shear view is that of a 5.0 caliber tangent ogive. The model axis system and sign conventions are illustrated in Figure 2. Note that x=0.0 occurs at the nose of the forebody with x increasing toward the model base. The cross-section is made up of tangent circular arcs with a 0.01 inch chine edge thickness.

The model is equipped with 91 surface static pressure taps arranged in 3 circumferencial rows and 3 raywise lines. At each of the circumferential rows (x/D = 1.0, 2.0 and 3.0), 15 pressure taps are distributed

Copyright © 1997, American Institute of Aeronautics and Astronautics, Inc.

across the leeward surface and 9 are distributed across the windward surface. The raywise lines are located along meridians of Φ = 120°, 180°, and 240° on the leeward surface. The internal pneumatic tubing is 0.032 inch inner diameter stainless steel.

The model was sting mounted horizontally on a three dimensional oscillation and positioning system (Figure 3). The oscillation system reduced the driving motor R.P.M. by a factor of 15 using a belt and pulley arrangement to produce model oscillation frequencies from 0 to 1 Hz. A cam was driven by the final pulley in the system to produce a continuous, sinusoidal model pitching motion with an amplitude of 52 degrees. A potentiometer was mounted to the system and was driven by a gear attached to the axle of the cam rocker arm. This potentiometer provided instantaneous model angle-of-attack measurement for both the static and dynamic cases.

The pressure data acquisition system consisted primarily of pneumatic tubing, electronically scanned pressure (ESP) modules, and a Pressure Systems Incorporated (PSI) System 8400 controller. The pressure modules were mounted to the main strut just under the tunnel floor. This location was chosen in order to minimize tube length and eliminate interference with the test section airflow. External pneumatic tubing was 22 inches long with an inside diameter of 0.032 inches. This diameter was the same as the stainless steel tubing which was internal to the model. This internal tubing varied in length from 1 to 10 inches. Therefore, the overall pneumatic tubing dimensions were 23 to 32 inches long. These tubing dimensions have been shown to provide excellent amplitude response and negligible phase lag at the frequencies tested.[8] This result was confirmed during this testing.[7]

Surface static pressure data were taken at essentially every degree angle-of-attack from 0° to 52°. These data were taken at a tunnel velocity of 200 ft/sec, which correspond to a Reynolds number, based on the 3-inch base diameter of the forebody, of 2.8×10^5. Oscillation frequencies from of 0 to 1 Hz., in 0.2 Hz. Increments, were tested. These frequencies correspond to reduced frequencies of 0 to 0.0137. Reduced frequency, defined by Eq. 1, was based on the 10.5 inch model length.

$$k = \omega l/2V_x \quad (l = \text{Model Length} = 10.5 \text{ in.}) \qquad (1)$$

Steady pressure data were the averaged result of 500 samples taken at a frequency of 50 samples per second. Unsteady pressure data were the result of ensemble averaging 10 complete oscillation cycles. These pressure data were integrated to provide both steady and unsteady force and moment data. As shown in Figure 4, the steady pressure integration results agreed very well with existing steady balance measurements.[9]

Flow visualization data were taken to determine the vortex system and help interpret the surface pressure data. Surface oil and smoke flow visualization were performed from 0 to 50 degrees angle-of-attack at 5 degree intervals for the steady case. Smoke flow visualization alone was used to capture flowfield images in the unsteady case. Still photographs (steady case only) and video were taken from above and from the side of the model. Both steady and unsteady smoke flow visualization was performed at a tunnel speed of 20 ft/sec ($R_e = 2.8\times10^4$). This value was chosen because it was the highest speed at which the primary vortical flowfield features were clearly visible.

The uncertainty associated with measured data was determined using the methods given in Coleman and Steele.[10] The uncertainty for angle-of-attack data was ±0.037°. Uncertainty in the integrated normal force was ±0.052. The uncertainty in the pressure coefficient data is given by equation 2.

$$w_{C_p} = \left(4.08\times10^{-5} + \left(3.66\times10^{-3}\cdot C_P\right)^2\right)^{1/2} \qquad (2)$$

This equation results in pressure coefficient uncertainties that range from $\pm4.08\times10^{-5}$ at pressure coefficients near zero, to $\pm1.60\times10^{-2}$ (or ±0.4%) at pressure coefficients around -4.0.

RESULTS AND DISCUSSION

The primary objective of this research was to establish the effects of an oscillatory pitching motion on the aerodynamics of a chined forebody. In order to determine these unsteady effects, a detailed knowledge of the steady aerodynamics and relationships between the flowfield and applied forces was essential. Existing steady research was augmented with additional steady data. The results of this combined steady research are summarized in this section along with the results of the unsteady research.

STEADY AERODYNAMICS

In order to complete the study of the steady aerodynamics of a chined forebody, existing steady research data were augmented with additional flow visualization and more complete surface static pressure data. This integrated database was analyzed to determine the nature of the steady flowfield and establish the relationships between this flowfield and the applied forces and moments. This research demonstrated that the sharp, highly swept leading edge of a chined forebody produced a steady windward flowfield at angle-of-attack (Figure 5) which was very

Copyright © 1997, American Institute of Aeronautics and Astronautics, Inc.

similar to that of a highly swept delta wing or a conventional elliptical cross-section forebody with the addition of a strake or a leading edge extension (LEX). The highly blended nature of the forebody also produced a steady leeward flowfield which was qualitatively similar to that of a body of revolution. These similarities in the steady flowfield translated into similarities in the effects of oscillatory pitching motion on the aerodynamics.

Figure 6 presents the right and left hand side primary vortex core trajectories as a function of angle-of-attack and longitudinal model station. This figure is a view looking aft, and each successive data point is 1 inch aft of the previous data point. Figure 7 through Figure 9 are photographs of the leeward surface oil flow visualization, taken at angles-of-attack of 20°, 30° and 40°. Each of these figures contain a top and a side view of the leeward surface.

Although at extremely low angles-of-attack there was no vortical flow present on the leeward side of the chined forebody, the primary vortices did begin to form, and generate vortex lift, at angles-of-attack as low as 5°. This early vortex formation resulted in a normal force curve with almost no low angle-of-attack linear region (Figure 4). By 10° angle-of-attack, three distinct leeward surface flowfield regions had developed on both the right and left sides of the forebody. A region of low energy streamwise flow was present along the centerline, where the existence of the leeward vortices had little effect on the surface flow. Outboard of this region, strong spanwise flow caused by primary vortex rotation was more dominant. Finally, a separated region existed along the chine edge, outboard of where the boundary layer associated with the strong spanwise surface flow had separated from the body surface.

As angle-of-attack increased from 10° to 20°, primary vortex strength and the surface area which was affected by vortical flow were steadily increasing while the primary vortex cores moved very slowly up off the forebody. As a result, the vortex lift built steadily and the center of pressure moved aft. This increasing vortex lift can be seen in Figure 4 as an increase in the normal force curve slope. In addition, the separated region along the chine edge, seen in Figure 7, grew progressively in width as the primary boundary-layer separation line moved inboard. As shown in Figure 10, this primary vortex boundary-layer separation occurred near a suction peak in the spanwise pressure distribution.

At around 20° angle-of-attack, the separated boundary layer under the primary vortex began to roll up into a counter-rotating secondary vortex. By 25° angle-of-attack, a secondary boundary-layer separation line appeared, on each side of the forebody, outboard of the primary separation line. This secondary separation line occurred at a second suction peak in the spanwise pressure distribution, and was associated with the inward boundary-layer flow under the secondary vortex. Between the primary and secondary separation lines, was a large separated region in which the spanwise pressure distribution was relatively constant and tertiary vortex formation appeared to take place. These relationships between boundary-layer separation and the spanwise pressure distribution are illustrated in Figure 10.

From 20° to 35° angle-of-attack, the boundary-layer separation lines progressed steadily inboard. This phenomena can be seen by comparing Figure 8 and Figure 9. In addition, the primary vortex cores moved rapidly up off the body over this angle-of-attack range, from the trailing edge forward (Figure 6). This rapid lifting off of the primary vortices was caused by secondary vortex formation and resulted in both a reduction in the development of vortex lift, shown in Figure 4, and a forward movement of the center of pressure. By 35° angle-of-attack streamwise centerline flow completely disappeared, and large streamwise pressure gradients began to develop on the leeward side of the body which eventually caused primary vortex burst. As shown in Figure 6, from 35° to 50° the primary vortex trajectories again moved more slowly up off the body with increasing angle-of-attack. This slower movement occurred because the secondary vortices were fully formed at this point.

The primary vortex burst points moved past the base of the body at around 38° and progressed steadily forward with increasing angle-of-attack until breakdown was essentially complete at around 58°.[9] The secondary vortices broke down just aft of the primary vortex burst point on the same side of the body. This secondary vortex breakdown can be seen in Figure 9, and occurred where the secondary separation line ended. Vortex breakdown eventually caused the normal force to decrease and the inward progression of the boundary-layer separation lines to stop. At around 58°, vortex breakdown was essentially complete and normal force began to decrease with increasing angle-of-attack.[9] This phenomena is analogous to stall on a wing or airfoil.

UNSTEADY AERODYNAMICS

The primary source of unsteady aerodynamic information used during this research was measured surface static pressure data. These data were used to examine the effects of reduced frequency on both the windward and leeward pressure distribution of the chined forebody surface. Unsteady smoke flow visualization was also performed to determine the effects of reduced frequency on the leeward vortical

Copyright © 1997, American Institute of Aeronautics and Astronautics, Inc.

flowfield of the chined forebody, and to help interpret the results of the unsteady pressure data. In addition, the unsteady pressure data were integrated to determine the effects of reduced frequency on the normal force and pitching moment.

Vortical Flowfield

Smoke flow visualization was performed at a Reynolds number of 2.8×10^4, based on the model base width of 3.0 inches. This Reynolds number corresponded to the highest velocity at which all features of the leeward vortical flowfield were clearly visible. The lowest possible oscillation frequencies of 0.0, 0.2 and 0.4 Hz were then used to produce reduced frequencies of 0, 0.0275, and 0.0550 based on the model length of 10.5 inches.

During the smoke flow visualization, steady and unsteady cases were run consecutively. Video tape footage of each case was taken at identical angles from above and from the side of the model. This footage was then compared directly to establish the effects of oscillatory pitching motion on the leeward vortical flowfield. The effect of reduced frequency on the primary vortex core position and burst point location are given in Figure 11 and Figure 12 respectively. It should be noted that the positive z direction is defined as upward in the body axis, as shown in Figure 2. In addition, 0% body length and 100% body length correspond to the model apex and model base respectively.

The vortex core positions, shown in Figure 11, were determined by locating the vertical center of the smoke trace induced by the vortex core. The vortex burst positions, shown in Figure 12, were determined by locating the point at which this smoke trace began to rapidly expand. At a given angle-of-attack in the steady case, the positions of these points were then compared to the known dimension of a model feature which was also visible in the steady video. This method resulted in steady vortex core and burst location data that compared very well with data extracted from existing laser sheet flow visualization.[9] Because of the uncertainties involved in both of these manual methods, the absolute position accuracy was relatively low. This accuracy was estimated to be around ±0.1 inches.

However, the relative position between the steady and unsteady positions was a far more important parameter in this analysis. This relative position was determined using a direct overlay of identical frames, which resulted in a relative position accuracy of around ±0.02 inches. The relative position data were then used as an increment to the steady vortex core and burst position data[9] to determine the unsteady position data plotted in Figure 11 and Figure 12. Therefore, the absolute positions shown in these figures are accurate to ±0.1 inches, but the relative positions are accurate to ±0.02 inches.

In the case of a pitching strake-wing configuration, Cunningham[11] found that the vortex position experienced a definite hysteresis in position during dynamic oscillations. The primary strake vortices were closer to the leeward surface during the dynamic upstroke and farther away during the dynamic downstroke than in the steady case. This same hysteresis behavior has been recorded on LEX-wing configurations.[2] During a dynamic upstroke, the LEX vortex was noticeably closer to the leeward surface than in the steady case.

A similar result was obtained during the current research on a chined forebody. As seen in Figure 11, the primary vortex was closer to the body during the dynamic upstroke than it was in the steady case. This result was not unexpected because as angle-of-attack increased in the steady case, the vortex moved progressively away from the body. During the dynamic pitch-up, this lifting-off process experienced some time delay which caused the vortex to be physically closer to body. Lateral vortex core position was essentially unaffected by dynamic pitching motion. This result was also expected since there was only a very small variation in lateral vortex position with changing angle-of-attack during the steady case.

It is apparent from Figure 11 that the magnitude of the difference between the steady and unsteady vortex core locations was far greater at 25° than it was at 35°, or at higher angles-of-attack. This 25° to 35° range, is the precise angle-of-attack range in which secondary vortex formation took place, and rapidly displaced the primary vortex up off the body during the steady case. During the dynamic upstroke, the secondary vortex actually formed at a lower angle-of-attack than in the steady case. However, there was a noticeable delay in the process of displacing the primary vortex.

By around 32° angle-of-attack, the dynamic primary vortex displacement process had completely "caught-up" to that of the steady case. Above 35°, the positional difference displayed more of a constant angle-of-attack lag behavior. This behavior is consistent with the gradual primary vortex lifting off process that took place after secondary vortex formation was complete during the steady case.

In addition to being closer to the body, the primary vortex core appeared to be "tighter" during the dynamic upstroke than in the steady case. This same result was obtained for a LEX-wing configuration. Brandon[27] observed that during the dynamic upstroke the LEX vortex was smaller and more stable than in the steady case. The decreased size, or increased tightness, along with the increased stability is characteristic of a more

Copyright © 1997, American Institute of Aeronautics and Astronautics, Inc.

coherent and energetic vortex. This suggests that the dynamic pitching motion altered the physical strength of the leeward primary vortex on both the chined forebody and the LEX-wing configuration.

As seen in Figure 12, there was also a definite hysteresis in primary vortex burst position during dynamic model oscillation. The figure shows that the dynamic burst position lagged the steady position by as much as 6° angle-of-attack during the upstroke, and 11° angle-of-attack during the downstroke. This is the same order of magnitude burst lag seen in past research conducted on other related configurations.[2,11,12] It is also interesting to note that at this reduced frequency the burst point always lags the steady position for the chined forebody. However, Bragg and Soltani noted that under some conditions, at low angles-of-attack, the unsteady burst point actually led the steady position on delta wings.[13]

As shown looking right to left in Figure 11, the primary vortex cores moved steadily toward the leeward surface of the body as angle-of-attack decreased in the steady case. During a dynamic pitch-down, this process presumably experienced some time delay which caused the vortex to be physically farther from the body than in the steady case. Results from Cunningham[11] reveal that this was the case for a dynamically pitching strake-wing configuration. This configuration had a very similar geometry to that of the chined forebody, and the primary vortices were noticeably farther from the body during the dynamic downstroke than in the steady case.

However, the current dynamic downstroke smoke flow visualization was inconclusive because the vortex was far more diffuse than during the steady case or during the dynamic upstroke. Furthermore, the primary vortices were burst over a much larger angle-of-attack range. These changes in the nature of the primary vortices made the precise location of the core extremely difficult to discern during the dynamic downstroke. In addition, the vortices were clearly lower in energy, and the energy was spread out over a much larger region, than in the dynamic upstroke.

Surface Static Pressure

Unsteady pressure data were taken at model oscillation frequencies of 0.0, 0.2, 0.4, 0.6, 0.8, and 1.0 Hz at tunnel speeds of 200 ft/sec. These combinations were used to produce reduced frequencies of 0.0, 0.0027, 0.0055, 0.0082, 0.0110, and 0.0137, based on the model length of 10.5 inches.

The effect of reduced frequency on an individual, leeward surface static pressure tap can be seen in Figure 13. During the upstroke, the identical "lifting" pressure occurred at a lower angle-of-attack as reduced frequency was increased. During the downstroke, the identical "lifting" pressure occurred at a higher angle-of-attack as reduced frequency was increased. The effect of reduced frequency on individual windward pressure taps was similar but far less pronounced. Again, the "lifting" pressure built-up more rapidly in the upstroke and unloaded more rapidly in the downstroke. This hysteresis illustrates the leading nature of the unsteady surface static pressure distribution.

The "kink" in this pressure curve, seen in Figure 13, was associated with the location of boundary-layer separation. As angle-of-attack was increased in the steady case, both the primary and secondary separation lines moved progressively inboard. After the primary separation line moved past a particular tap location, the tap was located in a separated region on the body surface, and the suction pressure stopped building as rapidly with increasing angle-of-attack. Subsequently, as the secondary separation line moved past a tap, the tap was located in an attached region under the secondary vortex, and the suction pressure began to build-up again with increasing angle-of-attack.

As reduced frequency was increased, this kink occurred at a lower angle-of-attack in the upstroke and at a higher angle-of-attack in the downstroke. This type of hysteresis indicates that both primary and secondary boundary-layer separation were leading in nature, during dynamic pitching motion. This result, confirmed by the early secondary vortex formation seen in the smoke flow visualization, was not surprising because the build-up of surface static pressure gradients caused the boundary-layer separation. During the dynamic pitching motion, these pressures gradients are also leading in nature.

Figure 14 and Figure 15 illustrate the effect of reduced frequency on both the leeward and windward surface static pressure distribution at 30° angle-of-attack. Figure 14 presents the leeward surface static pressure distribution for reduced frequencies of 0.0110 during the upstroke, 0.0055 during the upstroke, 0.0 (steady), 0.0055 during the downstroke, and 0.0110 during the downstroke. Figure 15 presents the windward surface static pressure distribution for the exact same conditions. Similarly, Figure 16 and Figure 17 illustrate the effect of reduced frequency on both the leeward and windward surface static pressure distribution at 40° angle-of-attack.

It should be noted that the pressure interpolation/extrapolation routine used throughout this research was developed primarily for the generation of highly accurate forces and moments. In order to provide the most accurate and repeatable data, all the available pressure data were used to compute the distributions, and any required extrapolations were linear. Because this premium was placed on the

Copyright © 1997, American Institute of Aeronautics and Astronautics, Inc.

integrated accuracy, some of the pressure distributions are not as smooth as possible. Specifically, the "hot spot" in the leeward, k=0.0055 pressure distribution (Figure 14), was caused by the linear extrapolation required to the chine edges. However, the contours are exact at all of the actual tap locations.

Windward surface static pressures and spanwise pressure gradients consistently increased as angle-of-attack was increased, in the steady case.[7] At low angles-of-attack, pressures were relatively low and spanwise pressure gradients were essentially non-existent. As angle-of-attack was increased to 20°, higher pressures had developed and distinct spanwise pressure gradients appeared. By 40° angle-of-attack (Figure 17), very high surface static pressures and pressure gradients had developed on the windward surface. These high pressures and pressure gradients, along with the high suction pressure on the leeward surface, drove the formation of the very strong leeward vortices.

These trends were exactly the same as those of pressure distributions at the same angle-of-attack and varying reduced frequency. For example, looking from right to left in Figure 15 and Figure 17, (k=0.0110 downstroke to k=0.0110 upstroke), the windward surface static pressures and spanwise pressure gradients progressively increased in the same manner as looking at a constant reduced frequency and increasing angle-of-attack. This illustrates the leading nature of the unsteady windward surface static pressure distribution.

The unsteady effects on the windward surface static pressure distribution were primarily an apparent mass phenomena. The low-speed windward flowfield of the chined forebody is fundamentally irrotational and incompressible, and there is no separated flow on the windward surface. In addition, the pressure distribution is sufficiently prescribed by assuming inviscid flow. Therefore, the windward flowfield is essentially potential, and the unsteady Bernoulli's equation can be used to provide qualitative guidance.

Equation 3 can be derived from the unsteady Bernoulli's equation following the method given by Katz,[14] and the solution to the potential equation of a closed body of revolution. The resulting equation is then the formula for the cross-flow contribution on the unsteady pressure of a pitching body in a steady, uniform, axial velocity flowfield (Figure 18). This cross-flow contribution is clearly the dominant term in the unsteady case.

$$p_{body} = \rho \cdot V_{\infty} \cdot \cos\alpha \cdot \left(\frac{\partial \alpha}{\partial t}\right) \cdot \cos\phi \cdot G(x) \qquad (3)$$

In this formula, G(x) is a function of the local geometry, and is always positive. For the windward surface, $\cos\phi$ is also positive. Therefore, for positive α and positive $\partial\alpha/\partial t$, the unsteady pressure contribution on the windward surface is positive. In other words, the windward side of a closed body in an unsteady, increasing cross-flow velocity field will experience a higher pressure than the same body in a steady velocity field of the same magnitude and direction. This apparent mass effect results in the leading nature of the unsteady windward surface static pressure distribution seen in Figure 15 and Figure 17. This leading effect produced higher windward surface static pressures and pressure gradients during the dynamic upstroke than in the steady case, and the opposite during the dynamic downstroke. These results were consistent with previous data taken on pitching prolate spheroids.[15,16]

The driving force behind the leeward surface static pressure distributions was the high suction pressures associated with the primary vortices. In general, the location of the primary vortex cores and the velocity profile within the primary vortices determines the entire leeward pressure field on this type of configuration. A stronger (higher rotation rates and/or core velocities) vortex will impart higher suction pressures on the leeward surface because of the higher velocities. Likewise, a primary vortex positioned closer to the body will also impart higher suction pressures on the leeward surface of the body since rotational velocity is inversely proportional to distance from the core.

In the steady case, vortical flow was present on the leeward side of the forebody at angles-of attack as low as 10° angle-of-attack.[7] This vortical flow imparted suction pressures along the chine edges, but had little effect on the centerbody. As angle-of-attack was increased to 30° (Figure 15), high suction pressures existed over much of the forebody span, and high spanwise pressure gradients had formed on the leeward surface. By 40° angle-of-attack (Figure 17), the entire leeward surface of the body was effected by vortical flow, and strong streamwise pressure gradients had begun to develop. It is important to note that the location of vortex burst could not be determined from these pressure distributions. However, the strong streamwise pressure gradients observed eventually caused the primary vortex to breakdown.

As seen in Figure 14 and Figure 16, the leeward surface static pressures also experienced a leading effect during dynamic pitch oscillations. At 20° angle-of-attack, high suction pressures existed along the chines in the k=0.0110 upstroke case, but only very low suction pressures existed in the downstroke. This indicates that strong vortical flow existed in the upstroke but not in the downstroke at 20° angle-of-attack for k=0.0110. As angle-of-attack was increased to 30° (Figure 14), very high suction pressures existed in the k=0.0110 upstroke case, and only moderate suction pressures existed in the downstroke. This leading effect was very similar in magnitude to that of

Copyright © 1997, American Institute of Aeronautics and Astronautics, Inc.

the windward surface static pressures. The pressure distribution from the k=0.0110 upstroke case (at a given angle-of-attack) looked very similar to that of the k=0.0055 upstroke case at a 5° higher angle-of-attack and the steady case at a 10° higher angle-of-attack.[7]

It was established above that the leeward vortex was closer to the body during the dynamic upstroke than in the steady case, and that the opposite was likely true during the dynamic downstroke. In addition, the increase in pressures on the windward surface during the dynamic upstroke, discussed above, caused a corresponding increase in the pressure differential between the leeward and windward surfaces. This increase in the pressure differential, together with the increase in the windward spanwise pressure gradients, would have driven the formation of stronger leeward vortices during the dynamic upstroke. These effects would have also resulted in weaker vortices during the dynamic downstroke.

The combination of stronger and closer primary vortices resulted in leeward surface static pressures building up more rapidly in the dynamic upstroke than in the steady case. Conversely, the combination of weaker and more removed primary vortices resulted in leeward surface static pressures unloading more rapidly in the dynamic downstroke than in the steady case. These effects on the unsteady flowfield were manifested in the leading effect seen in the leeward surface static pressure distributions.

Figure 19 through Figure 21 contain the leeward spanwise pressure distributions at 30° angle-of-attack for the same conditions as the previous figures. As reduced frequency was increased, the suction pressures increased over the entire measured span during the upstroke. As mentioned above, this increase was due to the increase strength and closer proximity of the leeward primary vortices. Because of the three-dimensional geometry of the chined forebody, the entire span was influenced by the vortex system at 30° angle-of-attack (Figure 8). This influence resulted in surface static pressures on both the chine area and the centerbody being impacted significantly by changes in the vortex flowfield.

In addition, the inboard suction peak moved noticeably inboard with increasing reduced frequency during the upstroke. This suction peak was associated with the point at which the boundary-layer under the primary vortex separated from the leeward surface. During the steady case, this point moved steadily inboard with increasing angle-of-attack. The fact that this point was farther inboard during the dynamic upstroke confirms the finding that unsteady secondary boundary-layer separation led the steady case.

During the dynamic upstroke, the spanwise point at which the leeward suction pressure began to sharply increase also moved inboard with increasing reduced frequency. In other words, the region of relatively low suction pressures, along the model centerline, decreased in span. The second spanwise suction peak appeared at a lower angle-of-attack with increased reduced frequency. This confirms that unsteady secondary vortex formation led the steady case, but that there was a lag in its ability to displace the primary vortex up off the body.

During the dynamic downstroke, increased reduced frequency resulted in decreased leeward surface suction pressures over the majority of the measured span. Again, the reduction in suction pressure was due to the decreased vortex strength and increased separation between the vortices and the leeward surface. In addition, a large portion of the span was affected because of the three-dimensional geometry of the chined forebody.

Integrated Forces and Moments

The measured surface static pressures, discussed in the previous section, were integrated using the procedure validated with existing steady balance data.[7] These integrated data were then used to determine the effects of an oscillatory pitching motion on the applied forces and moments at reduced frequencies of 0.0, 0.0027, 0.0055, 0.0082, 0.0110, and 0.0137. Figure 22 presents the effect of this reduced frequency variation on the integrated normal force.

This figure shows how the leading effect in both the leeward and windward surface static pressures translated into a leading effect in the integrated normal force. Normal force built-up faster in the upstroke and unloaded faster in the downstroke than in the steady case for all angles-of-attack. This leading effect resulted in a normal force hysteresis loop which increased in amplitude with increasing reduced frequency.

It is interesting to note that the location of the center of pressure was essentially unaffected by changes in reduced frequency. This result is consistent with the concept of a leading surface static pressure distribution, as the center-of-pressure variation with angle-of-attack was minimal in the steady case.

These results were very similar to those seen during previous research on similar configurations. Tests conducted on LEX-wing[12] and strake-wing[11] configurations undergoing rapid pitching oscillations also resulted in very large hysteresis loops in normal force and pitching moment at all angles-of-attack. However, Bragg and Soltani[3] demonstrated that for delta wings, significant normal force hysteresis loops existed only at angles-of-attack greater than about 15°, and these loops were smaller in amplitude than those of LEX-wing or strake-wing configurations.

Copyright © 1997, American Institute of Aeronautics and Astronautics, Inc.

In the case of the chined forebody, LEX-wing, and strake-wing configurations, strong vortical flow existed even at low angles-of-attack due to the very highly swept (80° - 90°), sharp leading edges. In addition, these configurations were highly three-dimensional with large diameter centerbodies and extensive areas of relatively small span. By contrast, the delta wing configuration had a flat leeward surface and a lower leading-edge sweep (70°), which resulted in weaker leading-edge vortices that formed at higher angles-of-attack. The combination of weaker vortices and a flat leeward surface resulted in the smaller dynamic effects on the delta wing, and an absence of low angle-of-attack force and moment hysteresis.

At most angles-of-attack the effect of increased reduced frequency acted as a pure phase shift on the normal force. However, at high angles-of-attack, there was more of a direct increase in maximum normal force during the dynamic upstroke, which was due to the lag in vortex breakdown. The phase shift effect was fairly linear over the range of reduced frequencies tested, but the maximum normal force increase seemed to diminish as a reduced frequency of 0.0137 was approached. This indicates that the vortex breakdown effects may have approached some change in state, or that the high deceleration rates required near the maximum angle-of-attack negated the increasing normal force effect. This type of diminishing reduced frequency effect has also been seen on highly swept delta wings.[17]

It is important to note that the effect of reduced frequency on the windward surface was at least as important to the integrated forces and moments as the effects on the leeward surface. Most previous research has concentrated exclusively on the reduced frequency effects on the leeward vortical flowfield, and in particular, the effects on primary vortex breakdown. However, this research clearly demonstrated that both the windward and leeward flowfields contributed to the integrated unsteady effects. More importantly, the state of the leeward vortex flowfield was directly related to the pressures and pressure gradients that existed in the windward flowfield. This research also showed that the effects of primary vortex strength and position were as important as the effects of vortex breakdown.

SUMMARY

An experimental investigation was conducted to examine the effects of an oscillatory pitching motion on the aerodynamics of a chined forebody. This study begins to fill the void between existing steady chined forebody data and unsteady research on related configurations. The effects of reduced frequency were investigated by running a range of model oscillation frequencies at a nominal Reynolds number. Surface pressures were measured at all conditions, and normal force and pitching moment were determined by integrating these data. Smoke and surface oil flow visualization techniques were utilized to determine the vortex system and help interpret the surface pressure data.

This research has revealed a great deal about both the steady and unsteady aerodynamics of the chined forebody. The results have also shed some light on previous research on similar configurations. The primary conclusions of this study were:

1. Viscous separation, which causes secondary vortex formation, was one of the most dominant flowfield features on the leeward surface of the chined forebody.[18] The secondary vortex influenced a large portion of the forebody surface and had a significant effect on the position of the primary vortex.

2. The windward surface static pressures and pressure gradients exhibited a leading effect during oscillatory pitching motion because of an apparent mass effect which was directly related to reduced frequency.

3. The leeward surface static pressures exhibited a leading effect during oscillatory pitching motion for several reasons. First, the leading effect in the windward pressures and pressure gradients resulted in a leading effect in primary vortex strength. Second, there was a lag in the secondary vortex displacement of the primary vortex, as well as a general lag in the primary vortex core's relative position with respect to the forebody. Finally, an appreciable lag existed in the vortex breakdown and re-formation process.

4. Integrated pressure data showed increased normal force in the upstroke and decreased normal force in the downstroke due to the leading effect in both the windward and leeward surface static pressure distributions.

ACKNOWLEDGEMENT

The authors wish to acknowledge Dr. Fred Roos, of McDonnell Douglas Aerospace, for his contributions to this work. Dr. Roos provided the wind tunnel model, and the existing steady data used in this research. He also provided his invaluable advice and expertise during every phase of the study.

Copyright © 1997, American Institute of Aeronautics and Astronautics, Inc.

REFERENCES

[1] Cunningham, A.M., Jr. and den Boer, R.G., "Analysis of Unsteady Force, Pressure and Flow-Visualization Data for a Pitching Straked Wing Model at High Angles of Attack," AGARD-CP-497, May 1991, pp. 8-1 to 8-16.

[2] Brandon, J. M. and Shah, G. H., "Unsteady Aerodynamic Characteristics of a Fighter Model Undergoing Large-Amplitude Pitching Motions at High Angles of Attack," AIAA-90-0309, Jan. 1990.

[3] Bragg, M.B. and Soltani, M.R., "Measured Forces and Moments on a Delta Wing During Pitch-Up," *Journal of Aircraft*, Vol. 27, No. 3, 1990, pp. 262-267.

[4] Taylor, L.K., Arabshahi, A. and Whitfield, D.L., "Unsteady Three-Dimensional Navier-Stokes Computations for a Prolate Spheroid Undergoing Time-Dependent Maneuvers," AIAA-95-0313, Jan. 1995.

[5] Roos, F.W. and Kegelman, J.T. , "Aerodynamic Characteristics of Three Generic Forebodies at High Angles of Attack," AIAA-91-0275, Jan. 1991.

[6] Robinson, M.C. and Wissler J.B., "Unsteady Surface Pressure Measurements on a Pitching Rectangular Wing," AIAA-88-0328, Jan. 1988.

[7] Mange, R.L., "Aerodynamics of a Chined Forebody Oscillating in Pitch," Ph.D. dissertation, University of Illinois at Urbana-Champaign, 1996.

[8] Chapin, W. G., "Dynamic-Pressure Measurements Using an Electronically Scanned Pressure Module," NASA Technical Memorandum 84650, July 1983.

[9] Kegelman, J.T. and Roos, F.W., "Influence of Forebody Cross-Section Shape on Vortex Flowfield Structure at High Alpha," AIAA-91-3250, Sept. 1991.

[10] Coleman, H.W., and Steele, W.G., *Experimentation and Uncertainty Analysis for Engineers*, John Wiley and Sons, Inc., New York, 1989, pp. 40-47.

[11] Cunningham, A.M., Jr., "Unsteady Low-Speed Wind Tunnel Test of a Straked Delta Wing, Oscillating in Pitch," Air Force Wright Aeronautical Lab, Wright-Patterson, AFB, OH, AFWAL-TR-87-3098, April 1988.

[12] Brandon, J.M., "Effects of Dynamic Stall Phenomena on High-Angle-of-Attack Characteristics of a Fighter Configuration," NASA-CP-3149, Oct. 1990, pp. 1039 to 1059.

[13] Soltani, M.R., Bragg, M.B. and Brandon, J.M., "Measurements on an Oscillating 70-Deg Delta Wing in Subsonic Flow," Journal of Aircraft, Vol. 27, No. 3, March 1990, pp. 211 to 217.

[14] Katz, J. and Plotkin, A., *Low-Speed Aerodynamics: From Wing Theory to Panel Methods*, McGraw-Hill, New York, 1991.

[15] Hoang, N.T., Wetzel, T.G. and Simpson, R.L., "Surface Pressure Measurements Over a 6:1 Prolate Spheroid Undergoing a Pitch-Up Maneuver," AIAA-94-1097, Jan. 1994.

[16] Hoang, N.T., Wetzel, T.G. and Simpson, R.L., "Unsteady Measurements Over a 6:1 Prolate Spheroid Undergoing Time-Dependent Maneuvers," AIAA-94-1908, June 1994

[17] Soltani, M.R., "An Experimental Study of the Relationship Between Forces and Moments and Vortex Breakdown on a Pitching Delta Wing," Ph.D. Dissertation, University of Illinois, 1992.

[18] Mange, R.L. and Bragg, M.B., "The Aerodynamics of a Chined Forebody Oscillating in Pitch," AIAA-95-1869, June 1995.

Copyright © 1997, American Institute of Aeronautics and Astronautics, Inc.

Figure 1: Wind Tunnel Model

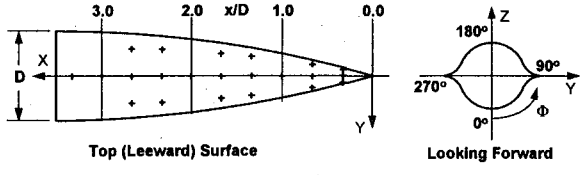

Figure 2: Model Coordinate System and Tap Locations

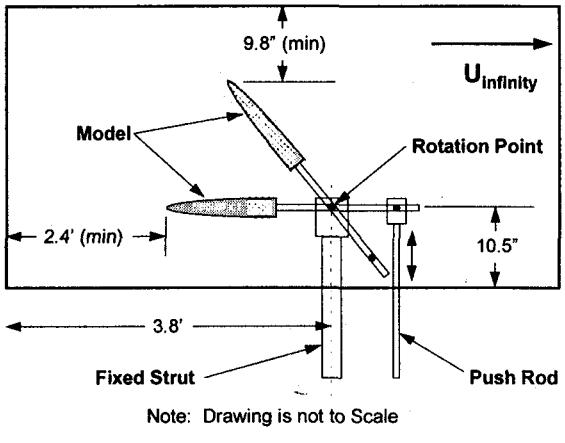

Figure 3: Model Position in Test Section

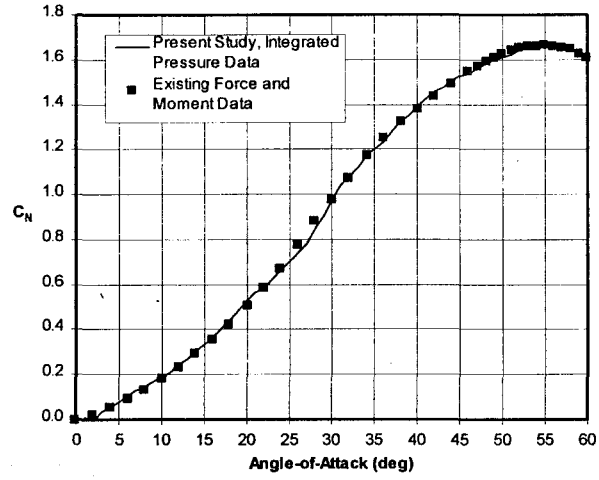

Figure 4: Steady Pressure Integration Results Vs. Existing Measured Data[5] (R_e = 280,000), $w_\alpha = 0.037°$, $w_{C_N} = 0.052$

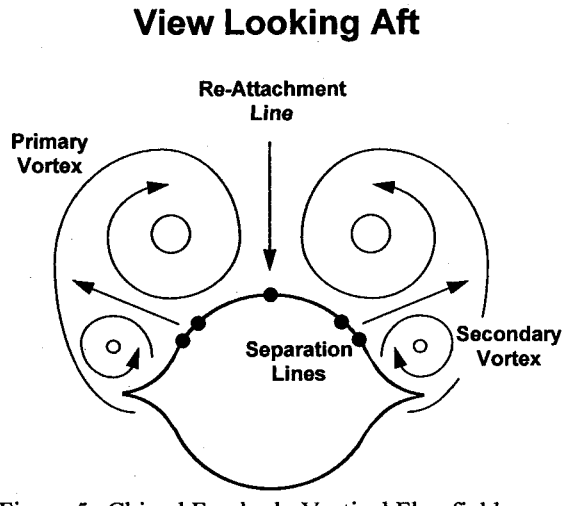

Figure 5: Chined Forebody Vortical Flowfield

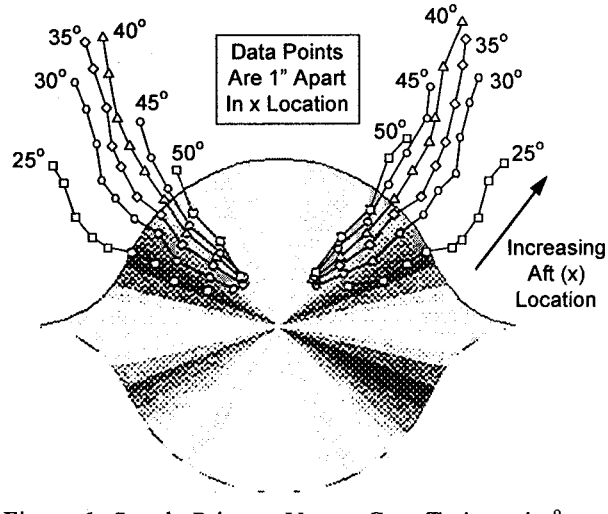

Figure 6: Steady Primary Vortex Core Trajectories[9]

Copyright © 1997, American Institute of Aeronautics and Astronautics, Inc.

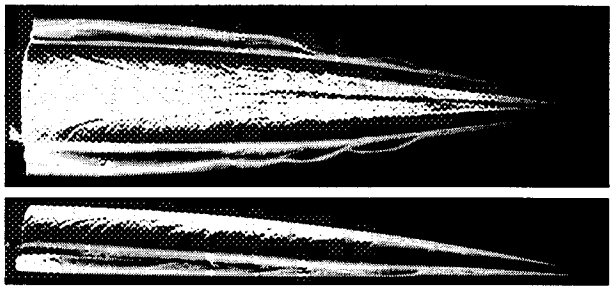

Figure 7: Steady Leeward Surface Oil Flow Visualization ($R_e = 210000$, $\alpha = 20°$)

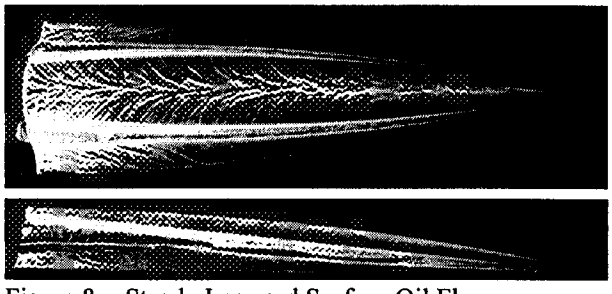

Figure 8: Steady Leeward Surface Oil Flow Visualization ($R_e = 210000$, $\alpha = 30°$)

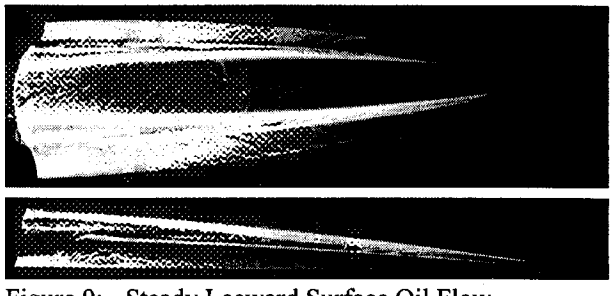

Figure 9: Steady Leeward Surface Oil Flow Visualization ($R_e = 210000$, $\alpha = 40°$)

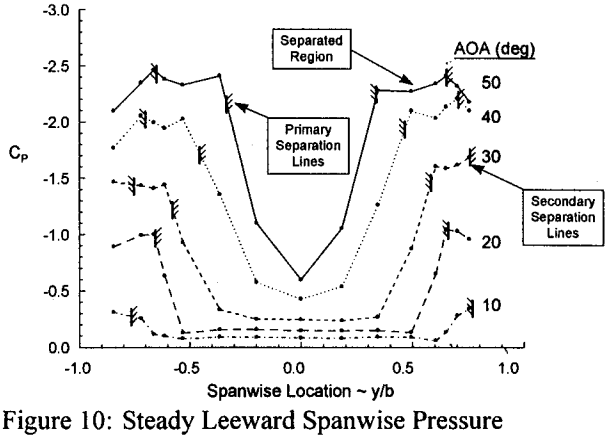

Figure 10: Steady Leeward Spanwise Pressure Distribution at x/l = 1.0 ($R_e = 280000$)

$$w_{C_P} = \left(4.08 \times 10^{-5} + \left(3.66 \times 10^{-3} \cdot C_P\right)^2\right)^{1/2}$$

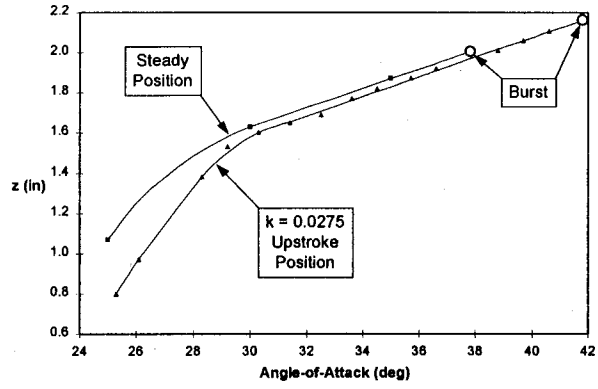

Figure 11: Effect of Reduced Frequency on Primary Vortex Core Position at Model Base ($R_e = 28000$), $w_z = \pm 0.10$ in, $w_{\Delta z} = \pm 0.02$ in, $w_\alpha = 0.037°$

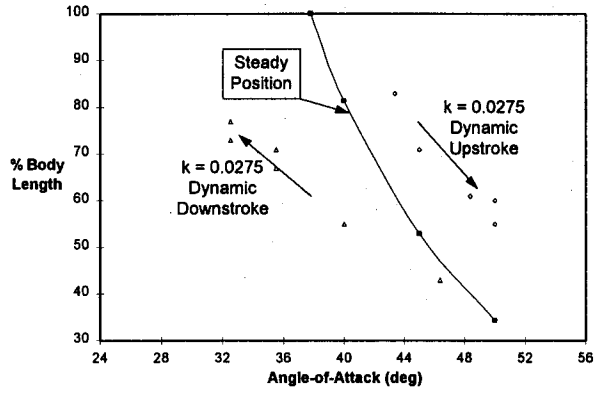

Figure 12: Effect of Reduced Frequency on Primary Vortex Burst Point Location ($R_e = 28000$), $w_z = \pm 0.10$ in, $w_{\Delta z} = \pm 0.02$ in, $w_\alpha = 0.037°$

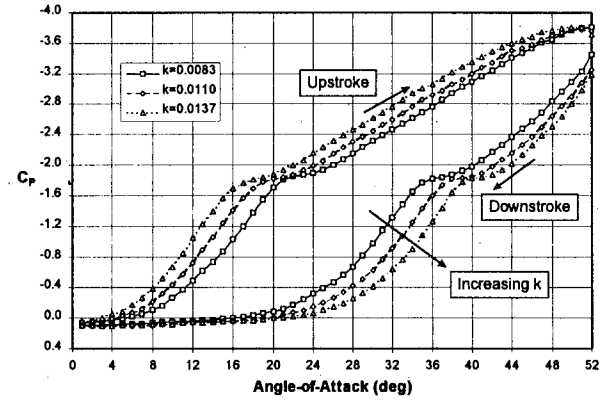

Figure 13: Effect of Reduced Frequency on a Forward Leeward Pressure Tap ($R_e = 280000$),

$$w_{C_P} = \left(4.08 \times 10^{-5} + \left(3.66 \times 10^{-3} \cdot C_P\right)^2\right)^{1/2},$$

$w_\alpha = 0.037°$

Copyright © 1997, American Institute of Aeronautics and Astronautics, Inc.

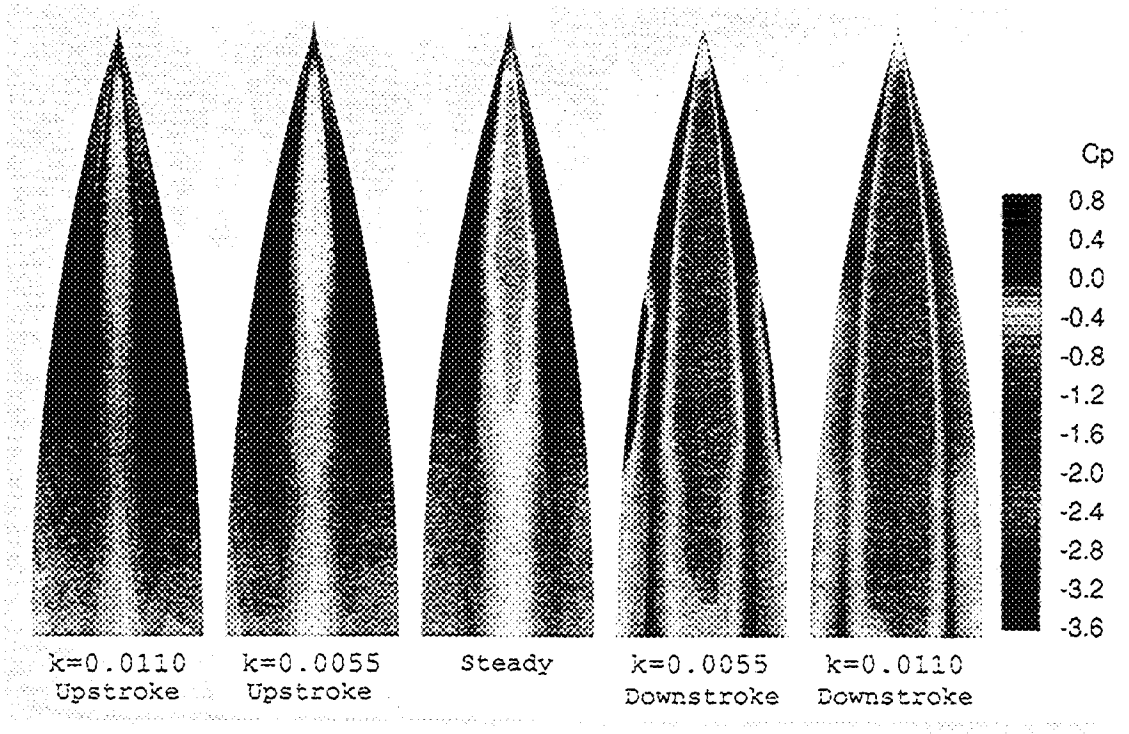

Figure 14: Effect of Reduced Frequency on Leeward Surface Static Pressure Distribution ($R_e = 280000$, $\alpha = 30°$), $w_{C_p} = \left(4.08 \times 10^{-5} + \left(3.66 \times 10^{-3} \cdot C_p\right)^2\right)^{1/2}$ at Tap Locations

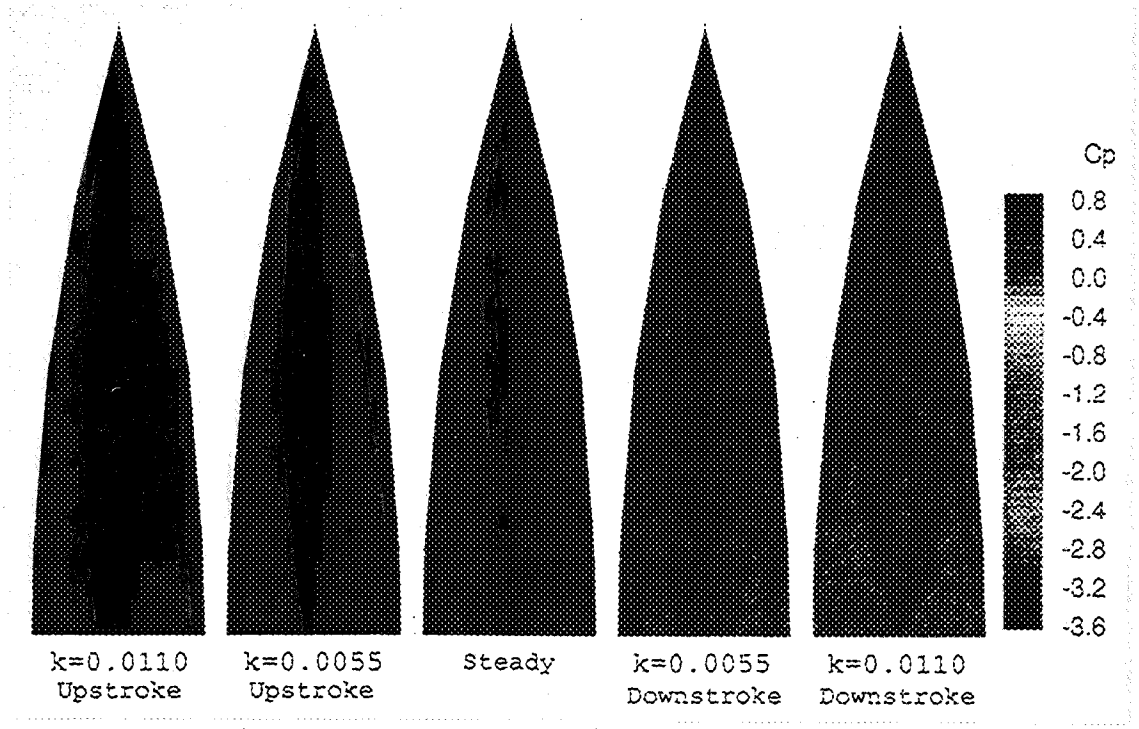

Figure 15: Effect of Reduced Frequency on Windward Surface Static Pressure Distribution ($R_e = 280000$, $\alpha = 30°$), $w_{C_p} = \left(4.08 \times 10^{-5} + \left(3.66 \times 10^{-3} \cdot C_p\right)^2\right)^{1/2}$ at Tap Locations

Copyright © 1997, American Institute of Aeronautics and Astronautics, Inc.

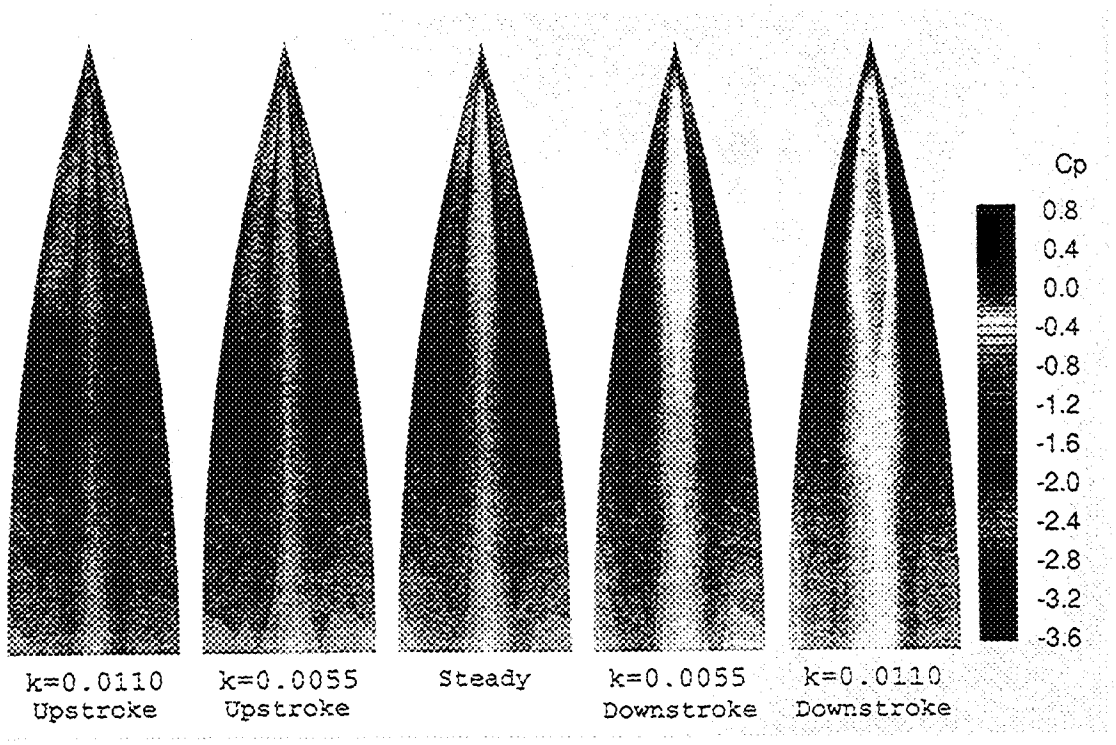

Figure 16: Effect of Reduced Frequency on Leeward Surface Static Pressure Distribution ($R_e = 280000$, $\alpha = 40°$), $w_{C_p} = \left(4.08 \times 10^{-5} + \left(3.66 \times 10^{-3} \cdot C_p\right)^2\right)^{1/2}$ at Tap Locations

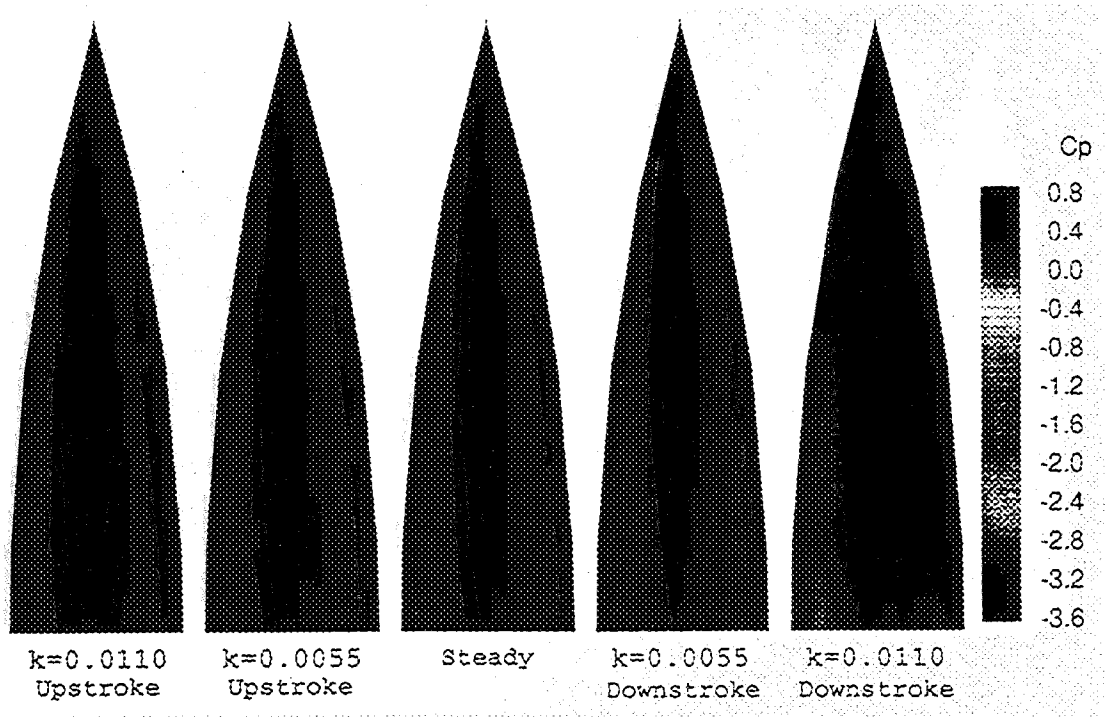

Figure 17: Effect of Reduced Frequency on Windward Surface Static Pressure Distribution ($R_e = 280000$, $\alpha =$ $w_{C_p} = \left(4.08 \times 10^{-5} + \left(3.66 \times 10^{-3} \cdot C_p\right)^2\right)^{1/2}$ at Tap Locations

Copyright © 1997, American Institute of Aeronautics and Astronautics, Inc.

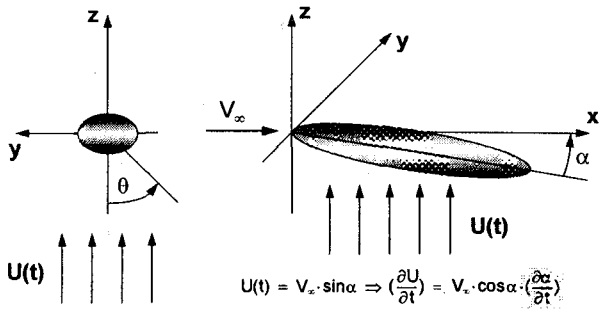

Figure 18: A Closed Body in an Unsteady, Increasing, Cross-Flow Velocity Field

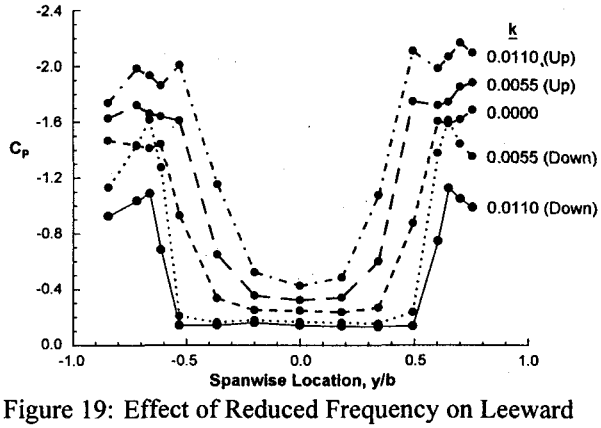

Figure 19: Effect of Reduced Frequency on Leeward Surface Static Pressure Distribution, $\alpha = 30°$, $x/d = 1.0$, $R_e = 280000$,

$$w_{C_P} = \left(4.08 \times 10^{-5} + \left(3.66 \times 10^{-3} \cdot C_P\right)^2\right)^{1/2}$$

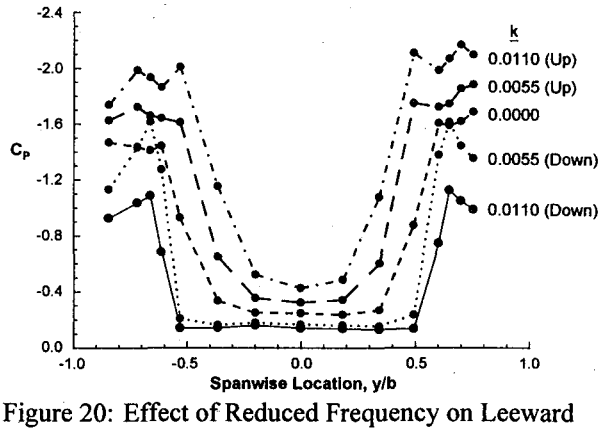

Figure 20: Effect of Reduced Frequency on Leeward Surface Static Pressure Distribution, $\alpha = 30°$, $x/d = 2.0$, $R_e = 280000$,

$$w_{C_P} = \left(4.08 \times 10^{-5} + \left(3.66 \times 10^{-3} \cdot C_P\right)^2\right)^{1/2}$$

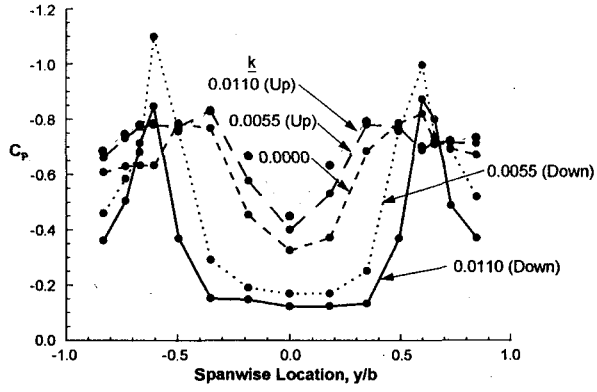

Figure 21: Effect of Reduced Frequency on Leeward Surface Static Pressure Distribution, $\alpha = 30°$, $x/d = 3.0$, $R_e = 280000$,

$$w_{C_P} = \left(4.08 \times 10^{-5} + \left(3.66 \times 10^{-3} \cdot C_P\right)^2\right)^{1/2}$$

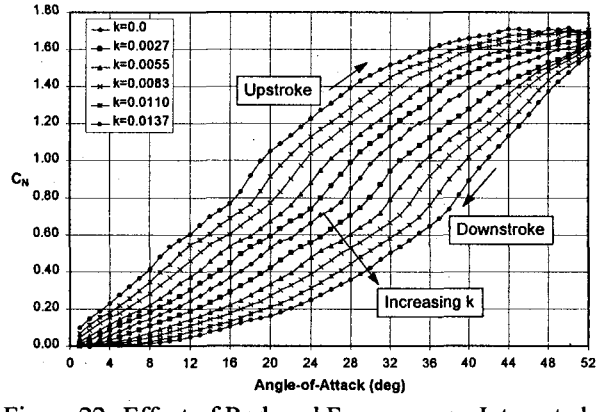

Figure 22: Effect of Reduced Frequency on Integrated Normal Force (R_e=280,000), $w_\alpha = 0.037°$, $w_{C_N} = 0.052$